Fatigue properties of metal matrix syntactic foams

I. N. Orbulov, B. Katona, G. Szebényi,
Budapest University of Technology and Economics, Faculty of Mechanical Engineering, Department of Materials Science and Engineering, Budapest
MTA–BME Research Group for Composite Science and Technology, Budapest

1 Introduction

Closed cell, high strength metallic foams, as ceramic hollow sphere reinforced metal matrix syntactic foams (MMSFs) are promising materials to build lightweight structural parts. The application of these composites can range from load bearing structures to vibration damping structural parts like machine beds, spindles etc. In numerous cases, the fatigue properties are necessary in order to conduct proper design calculations.

The basic mechanical properties of MMSFs have been widely studied. The publications focus mainly on the compressive behavior of the foams (as most common loading mode), but tensile and wear properties [1, 2] as well as structure reconstruction methods [3] have been described too. For example, the quasi-static and high-strain-rate properties of Al-Al_2O_3 MMSFs were monitored and predicted considering the strength of the matrix material and the size of the reinforcing hollow spheres [4-6]. Peroni, Lehmhus, Weise et al. [7-10] characterized iron based syntactic foams reinforced by glass microspheres. Besides the production, the quasi-static tensile / compressive properties and the strain-rate dependency of the materials were investigated up to the dynamic loading rates (in overall from 10^{-3} s^{-1} up to 10^{3} s^{-1}). The results demonstrated that the strain-rate influence observed for the syntactic foam was mainly correlated to the matrix. Taherishargh et al. [11, 12] investigated the application possibility of low-density perlite as filler material in order to reduce the production costs. Owing to the high porosity of the filler material (~95%), the total porosity of the new foam reached ~60%. Under compression, the MMSFs showed common stress–strain curves consisting of elastic, plateau and densification regions. Because of their consistent plateau stress (average value ~30 MPa), large densification strain (almost 60%), and high-energy absorption efficiency (~90%) the produced MMSFs are effective energy absorbers. Besides the above mentioned and similar works, only a little effort was focused on the fatigue properties.

Vendra et al. investigated the fatigue properties of MMSFs that contained steel hollow spheres in aluminum matrix (made by gravity casting) or in steel matrix (made by powder metallurgy method). Under cyclic compression loading, the MMSFs showed high cyclic stability and the deformation of the composite foam samples could be divided into three stages – linear increase in strain with fatigue cycles (stage I), minimal strain accumulation in large number of cycles (stage II) and rapid strain accumulation within few cycles up to complete failure (stage III). The deformation of the MMSFs occurred to be uniform compared to regular metal foams, which deform by forming collapse bands at weaker sections [13].

Somewhat similar, but not identical case is the assembled pack of hollow spheres (without the surrounding matrix) that called hollow spheres structures (HSS) were investigated by Caty et al. The steel specimens were tested in both cyclic compression and tension modes. The re-

sults showed that the constitutive material and in particular, the processing route had the most dominant effect on fatigue properties through the wall properties, the shape and strength of the bonding between two spheres and the homogeneity of the resulting material. The density of the structure was a secondary important parameter. The diameter of the spheres had a minor effect on fatigue strength, but acted more on the fatigue stress sensibility (slope of the S–N curve). Moreover, the fatigue limit in tension loading was found to be twice lower than in compression loading [14].

2 Materials and methods

The investigated MMSFs were produced by inert gas pressure assisted, liquid state infiltration. In this commonly used process Ar gas was used as inert pressurizing medium. The chemical compositions of the applied matrix materials are listed in Table 1.

Table 1. Measured chemical composition of the applied matrix materials.

Matrix	Composition (wt%)						
	Si	Fe	Cu	Mn	Mg	Zn	Al
Al99.5	0.123	0.328	0.003	0.003	0.002	0.005	Rem.
AlSi12	12.830	0.127	0.002	0.005	0.010	0.007	

As filler, SL300 grade ceramic hollow spheres (Table 2) were applied from Envirospheres Pty. Ltd. The volume fraction of the filler was always maintained at ~65 vol%. The hollow sphere consisted of 33 wt% Al_2O_3, 48 wt% amorph SiO_2 and 19 wt% mullite ($Al_2O_3 \cdot SiO_2$).

Table 2. Typical average properties of hollow ceramic microspheres.

Outer diameter (μm)	Wall thickness (μm)	Strength (MPa)	Real density (kgm^{-3})
150	6.75	~45	691

The fatigue tests were performed on an Instron 8872 type servo-hydraulic universal testing machine in a four bar guided tool. The plates of the tool were ground and tempered to 45 HRC. The specimens were cylindrical (Ø8.50 mm × 12.75 mm, the aspect ratio was H/D = 1.5). The loading of the specimen was cyclic compression with R = 0.1 at different load ratios ($k = \sigma_{max} / \sigma_c$) from 0.6 up to 0.9. The frequency of the cycles was set to f = 10 Hz. Five specimens were tested on each load ratio and the measurements were statistically evaluated. As failure criterion a deformation limit was applied, the specimen considered to be broken if its overall engineering deformation reached $\varepsilon = 2\%$. In other cases, the tests were stopped at $2 \cdot 10^6$ cycles and the specimens survived the test.

3 Results and discussion

A typical, quasi-static compressive engineering stress – engineering strain curve of an AlSi12-SL300 MMSF is shown in Fig. 1a. The curve can be divided into three parts and more subparts, as it was analyzed and detailed previously [15-17]. According to the ruling standard about the compressive tests of cellular materials [18], the curve has several characterizing properties. Besides others, the characterizing properties are the compressive strength (σ_c), the fracture strain (ε_c), the structural stiffness (S) and the absorbed mechanical energy (W_c). In the

actual point of view, only the compressive strength (σ_c (MPa)) is important as it gives the base for the definition of the load ratio (k), or normalized stress level. Based on the load ratio, the cyclic loading is depicted in Fig. 1b. As the MMSF blocks can have gradients in their physical and mechanical properties [19], resulting in significant scatter in their compressive strength, the average values cannot be used as the base for the load ratio with full confidence (especially in the case of high load ratios, near to the compressive strength). Therefore, during the turning, a pair of specimens was machined from very next places to each other. The method ensured identical compressive strength for the specimen pairs. The first specimen was used to preliminary measure the compressive strength and the second one was subjected to the cyclic loading based on the preliminary test.

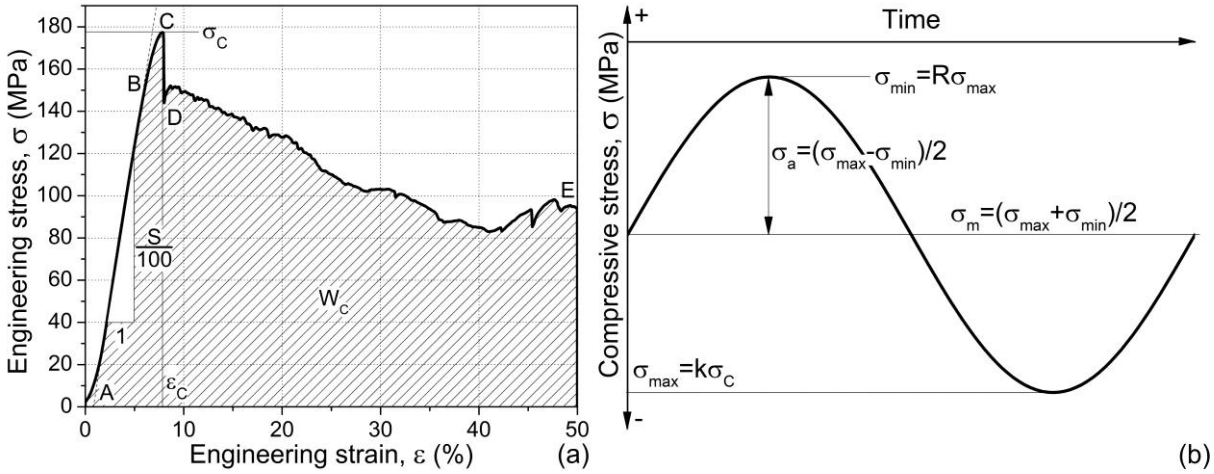

Figure 1. Typical quasi-static compressive curve of an AlSi12-SL300 MMSF (a) and the applied cyclic loading (b).

During the cyclic loading, the cycles were recorded and evaluated for the overall (elastic and plastic) maximal compressive deformation that was plotted against the number of cycles. When the overall deformation reached 2% the tests were stopped and the specimen considered to be failed. A typical deformation – number of cycles curve is plotted in Fig. 2a.

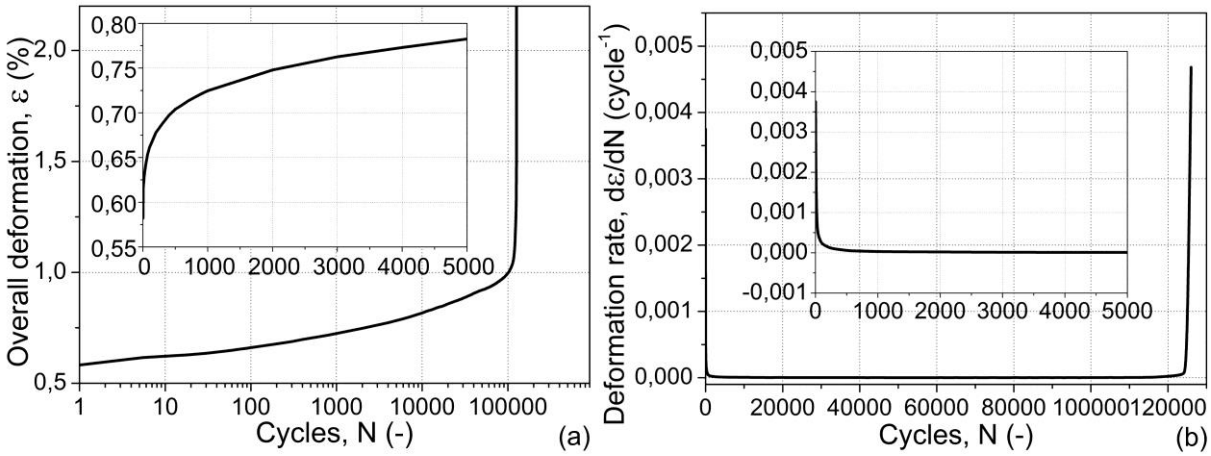

Figure 2. Typical deformation versus cycles (a) and deformation rate versus cycles (b) curve of an AlSi12-SL300 MMSF at load ratio k = 0.7.

As it is shown in the inset diagram of Fig. 2a, the cyclic deformation starts with a rapid deformation accumulation, the overall deformation increased quickly, up to about 1000 cycles. Parallel to, this the deformation rate decreased sharply (very left side and inset graph in

Fig. 2b). Subsequently, the deformation rate gradually decreased further and became constant. For a long term the deformation rate (e. g. the increment of deformation cycle by cycle, or the slope of the overall deformation versus cycles curve) was practically 0 $cycle^{-1}$. After a quite long and constant part, the deformation rate increased dramatically and the deformation accumulated rapidly. Finally, the specimen was broken (at $\varepsilon = 2\%$) or survived $2 \cdot 10^6$ cycles and the test was stopped. The repeated tests were evaluated by the method of Weibull fittings and lifetime approximations at different load ratios. The probability of survival was set to 80% and linear fittings were performed in order to get continuous connection between the load ratio (or normalized stress) and the expected lifetime. The evaluated data for the investigated matrix and hollow sphere combinations with the corresponding error bars are shown in Fig. 3.

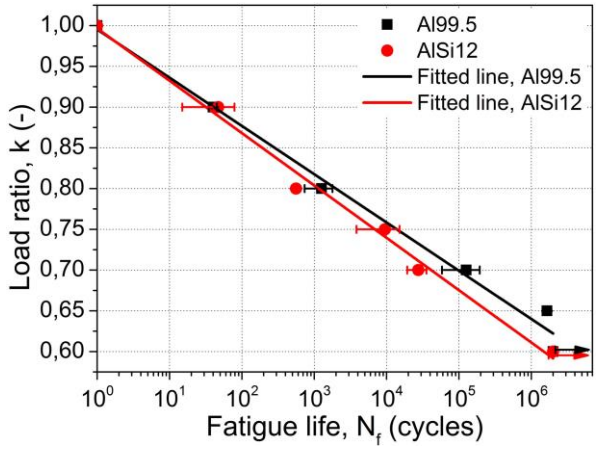

Figure 3. Load ratio versus fatigue life curves of the investigated MMSFs.

As it can be seen in Fig. 3, the fitted lines starts from the same point, corresponding to the normalized quasi-static compressive strength of the material (one cycle, k = 1 loading ratio). With the decrement of the load ratio, the fatigue life increased simultaneously. The gradually increasing deviation between the fitted lines corresponds to the different failure mechanism in the case of Al99.5 and AlSi12 matrix materials respectively, and it is influenced by the probabilistic nature of the crack initiation mechanism (especially at lower load ratios). The softer, unalloyed matrix ensured higher fatigue life, thanks to the large deformation capability of the pure Al matrix. The near eutectic, Si alloyed matrix showed lower fatigue life, due to the presence of Al and Si lamellae and in some places primary Si precipitations (see Table 1, the eutectic formed at 12.6 wt% Si [20]). In Fig. 4 a typical micrograph of an AlSi12 MMSF is shown, with its eutectic microstructure and a large, blocky Si precipitation.

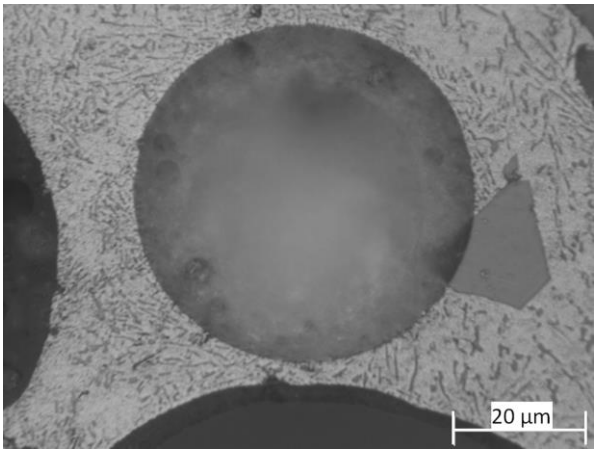

Figure 4. Micrograph of AlSi12 MMSF showing eutectic microstructure and a blocky precipitation.

The Si lamellae and the edges of the primary Si precipitations act as stress concentrators sites and they can be the starting points of microcracks. The difference can also be observed in the failure mechanism. In quasi-static compression and in the case of H/D = 1.5, two typical failure mechanism could be separated [15-17]. In the case of Al99.5 matrix, the soft base material deforms plastically and the typical failure mechanism is shearing induced cleavage, in which usually one determined shear band is formed, closing ~30-40° to the load direction. The initiation of the cleavage band depends on the crush strength of the hollow spheres. In the case of harder, Si alloyed matrix the failure concentrates between two compression cones forms on the tool plates. The shape of the failure zone is usually lenticular combined with shear bands at its perimeter. This failure mode is ruled by the yield strength of the matrix.

In cyclic compression the failure modes (Fig. 5) depends on the relation between the strengths of the matrix and the ceramic hollow spheres. If the matrix yields before the compressive stress reaches the crush strength of the hollow spheres, the deformation accumulates by the plastic deformation of the matrix until the cleavage band formed in the weakest region (Fig. 5a). This can easily occur at critical sites in the matrix walls and struts (between the hollow spheres), in which multiaxial (compression, tension and bending) stress state exists due to the built up of the foam structure. Later, the deformed band thickens and the failure criterion is reached quickly. In other case, when the hollow spheres crushes before the matrix yields, a lenticular damaged zone forms in the center region of the specimen (Fig. 5b). Near the collapsed hollow spheres the matrix deforms plastically (the support of the ceramic hollow sphere is lost), the matrix slowly compresses the broken spheres and replaces its cavity. Due to this process, the overall deformation accumulates quickly.

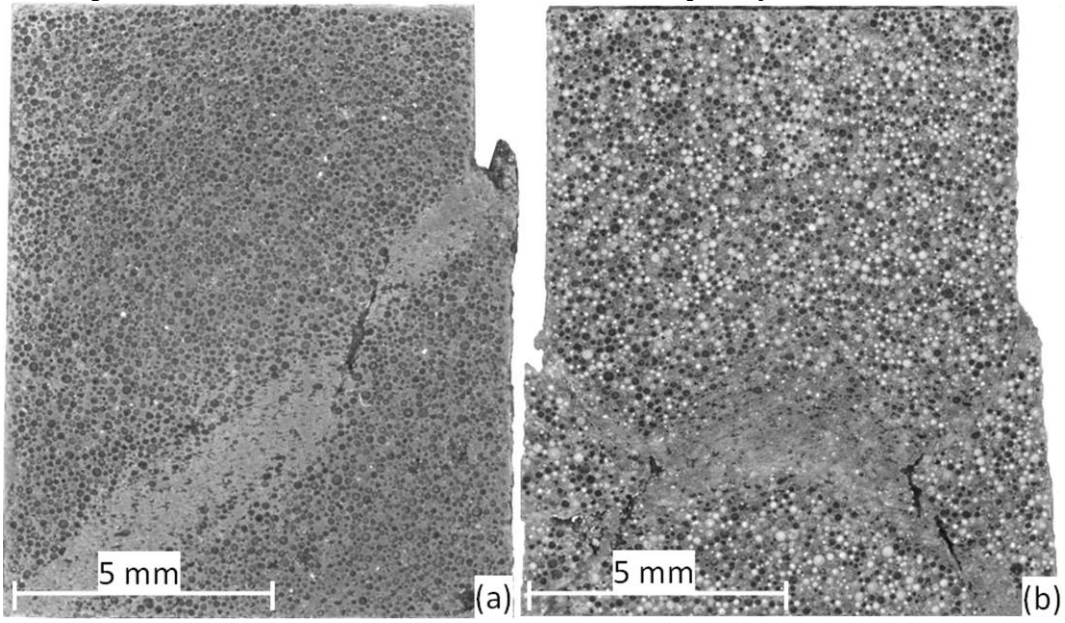

Figure 5. Macrograph of broken (a) Al99.5 and (b) AlSi12 MMSF.

4 Conclusions

From the above detailed investigations, the following conclusions can be summarized.

- The deformation versus number of cycle curves of MMSFs can be divided into three separate sections. In the first part rapid deformation accumulation occurs; the longest part is

the second one, during which the deformation rate is practically zero and finally the third part's rapid deformation results in failure.

- The matrix material has significant effect on the expected lifetime of the MMSFs at given load ratio (normalized stress levels). The softer matrix ensure longer lifetime. The lifetime gap between the different MMSFs increases as the load ratio decreases.
- The failure mode of MMSFs is also influenced by the matrix material and depends on the ratio between the yield strength of the matrix and the crush strength of the ceramic hollow spheres.

5 Acknowledgements

This paper was supported by the János Bolyai Research Scholarship of the Hungarian Academy of Sciences. (I. N. Orbulov and G. Szebényi.)

6 References

[1] K. Májlinger, Bányászati és Kohászati Lapok – Kohászat (Wear behavior of hybrid syntactic foams, in press, in Hungarian).
[2] B. Bozóki, K. Májlinger, in Proceedings of XXII. Nemzetközi Gépészeti Találkozó, ed. V. J. Csibi, Nagyszeben, Romania, p. 62-65. (in Hungarian).
[3] I. Kozma, I. Zsoldos, G. Dorogi, S. Papp, Period. Polytech. Mech. Eng. 2014, 58, 87-91.
[4] J. A. Santa Maria, B. F. Schultz, J. B. Ferguson, P. K. Rohatgi, Mater. Sci. Eng. A. 2013, 582, 415-422.
[5] J. B. Ferguson, J. A. Santa Maria, B. F. Schultz, P. K. Rohatgi, Mater. Sci. Eng. A. 2013, 582, 423-432.
[6] J. B. Ferguson, J. A. Santa Maria, B. F. Schultz, N. Gupta, P. K. Rohatgi, J. Mater. Sci. 2014, 49, 1267-1278.
[7] J. Weise, D. Lehmhus, J. Baumeister, R. Kun, M. Bayoumi, M. Busse, Steel. Res. Int. 2013, 85, 486-497.
[8] L. Peroni, M. Scapin, M. Avalle, J. Weise, D. Lehmhus, J. Baumeister, M. Busse, Adv. Eng. Mater. 2012, 14, 909-918.
[9] L. Peroni, M. Scapin, M. Avalle, J. Weise, D. Lehmhus, Mater. Sci. Eng. A. 2012, 552, 364-375.
[10] L. Peroni, M. Scapin,, C. Fichera, D. Lehmhus, J. Weise, J. Baumeister, M. Avalle, Compos. Part B. 2014, 66, 430-442.
[11] M. Taherishargh, I. V. Belova, G. E. Murch, T. Fiedler, Mater. Sci. Eng. A. 2014, 604, 127-134.
[12] M. Taherishargh, I. V. Belova, G. E. Murch, T. Fiedler, Mater. Des. 2014, 63, 375-383.
[13] L. Vendra, B. Neville, A. Rabiei, Mater. Sci. Eng. A. 2009, 517, 146-153.
[14] O. Caty, E. Maire, T. Douillard, P. Bertino, R. Dejaeger, R. Bouchet, Mater. Lett. 2009, 63, 1131-1134.
[15] I. N. Orbulov, J. Ginsztler, Compos. Part A. 2012, 43, 553-561.
[16] I. N. Orbulov, Mater. Sci. Eng. A. 2012, 555, 52-56.
[17] I. N. Orbulov, J. Ginsztler, Acta Polytech. Hungarica. 2012, 9, 43-56.
[18] DIN 50134 Testing of metallic materials - Compression test of metallic cellular materials (2008). DIN 50134 Testing of metallic materials - Compression test of metallic cellular materials (2008).
[19] K. Májlinger, I. N. Orbulov, Mater. Sci. Eng. A. 2014, 606, 248-256.
[20] Binary alloys phase diagrams, 2nd ed., ASM International, 1990, p. 211.